Soft Matter

Accepted Manuscript

This article can be cited before page numbers have been issued, to do this please use: D. Zhao, Q. Tang, Q. Zhou, K. Peng, H. Yang and X. Zhang, *Soft Matter*, 2018, DOI: 10.1039/C8SM01575A.

ROYAL SOCIETY OF CHEMISTRY

rsc.li/soft-matter-journal

View Article Online
DOI: 10.1039/C8SM01575A

Journal Name

ARTICLE

A photo-degradable injectable self-healing hydrogel based on star poly(ethylene glycol)-*b*-polypeptide as potential pharmaceuticals delivery carrier

intReceived 00th January 20xx,
Accepted 00th January 20xx

DOI: 10.1039/x0xx00000x

www.rsc.org/

Dinglei Zhao,[a] Quan Tang,[a] Qiang Zhou,[a] Kang Peng,[a] Haiyang Yang*,[a] and Xingyuan Zhang*[a]

As one of the most promising biomaterials, injectable self-healing hydrogels have found broad applications in a number of fields such as local drugs delivery. However, the controlled release of drugs in hydrogels is still difficult to realize up to now. Here, we report a novel photo-degradable injectable self-healing hydrogel based on the hydrophobic interaction of a biocompatible four-arms star polymer, poly(ethylene glycol)-*b*-poly(*γ*-o-nitrobenzyl-*L*-glutamate). The hydrophobic interaction between poly(*γ*-*o*-nitrobenzyl-*L*-glutamate) not only connects poly(ethylene glycol)-*b*-poly(*γ*-*o*-nitrobenzyl-*L*-glutamate) together as a crosslink but also provides a hydrophobic domain to encapsulate hydrophobic pharmaceuticals such as Doxorubicin (DOX). Due to the dynamic character of the hydrophobic interaction, the hydrogel exhibits excellent injectable and self-healing ability. In particular, the photolabile *o*-nitribenzyl ester group is cleaved under UV irradiation. As a result, the hydrophobic domain transforms into the hydrophilic one and the DOX embedded is released effectively. The increasing release ratio of Dox dramatically enhances the apoptosis ratio of HeLa cell. We expect these attractive properties maybe beneficial to the practical application of hydrogel as an effective local drugs delivery in a truly physiological environment.

Introduction

Hydrogels are a sort of attractive soft materials[1, 2] because of their considerable practical potential for biomedical and pharmaceutical applications[3-5]. In particular, injectable self-healing hydrogels[5-12], which can be implanted through a syringe at the targeted sites and then rapidly form bulk gels in situ, have been paid much attention in recent researches.

To date, many works about 3D injectable self-healing hydrogels have been reported. The methods of fabricating injectable self-healing hydrogels are generally categorized into three types: physical cross-linking,[13-18] dynamic chemical cross -linking[19-22] or the dual mechanism.[19, 23] Among all methods, physical cross-linking is the most commonly used due to the dynamical self-adaptation. For instance, Leong et al.[24] reported an injectable hydrogel formed from poly(ethylene oxide)s and α-cyclodextrin for drug delivery. The hydrogel formation was based on physical crosslinking induced by supramolecular self-assembling. Pochan et al.[25] demonstrated an injectable hydrogel based on curcumin-loaded β-sheet assembling peptide nanofiber hydrogels for local chemotherapy. Although many injectable self-healing hydrogels have been designed in drug delivery, the release mechanism of the carriers is passive material degradation. Therefore, it is still a challenge to active control the release of drugs on demand in injectable self-healing hydrogels.

Active controlling release can efficiently optimize the pharmacokinetic of drugs and reduce the amount of necessary drugs. The convenience of fewer and more effective doses also increases patient compliance.[26] Stimuli-responsive hydrogels have advantages in realizing on demand controlled release of payloads.[27] A variety of stimuli including pH,[4, 28, 29] redox species,[4] photo-irradiation,[30] enzymes[31] have been applied to accomplish on demand release of payloads. Among all stimuli, light is of particular fascinating stimulus to manipulate the properties of hydrogels as it is a remote stimulus that can be controlled spatially and temporally with great ease and convenience.[32-39] Hence, photo responsive injectable self-healing hydrogels are ideal on demand release carriers.

In recent years, biodegradable polypeptides have been proposed to design stimuli-responsive injectable hydrogels, due to their hierarchical self-assembly,[40] multiple secondary,[41] biocompatibility[42] and biodegradability.[43] Deming et al.[44] reported a photo-degradable copolypeptide hydrogel which included charged amino acid residues for better water solubility. The charges, especially positive charges, may cause inevitable side effects such as unfavourable protein absorption

[a] CAS Key Laboratory of Soft Matter Chemistry, School of Chemistry and Materials Science, University of Science and Technology of China, Hefei, 230026, P. R. China. E-mail: yhy@ustc.edu.cn; zxym@ustc.edu.cn.

† Footnotes relating to the title and/or authors should appear here.

Electronic Supplementary Information (ESI) available: [details of any supplementary information available should be included here]. See DOI: 10.1039/x0xx00000x

View Article Online
DOI: 10.1039/C8SM01575A

in vivo. Hence, non-ionic poly(ethylene glycol) (PEG) is a superior choice as hydrophilic block, especially 4-arm PEG which has attracted extensive attention due to its perfect spatial structure,[21, 45, 46] dissolubility and biocompatibility.[47]

Here, we designed a photo-degradable injectable self-healing hydrogel based on the hydrophobic interaction of a biocompatible four-arms star polymer, poly(ethylene glycol)-*b*-poly(*γ*-*o*-nitrobenzyl-*L*-glutamate). The hydrophobic interaction between poly(*γ*-*o*-nitrobenzyl-*L*-glutamate) not only connects poly(ethylene glycol)-*b*-poly(*γ*-*o*-nitrobenzyl-*L*-glutamate) together as a reversible crosslink but also provides a hydrophobic domain to encapsulate hydrophobic pharmaceuticals such as Doxorubicin (DOX). Upon irradiation, the full cleavage of *o*-nitrobenzyl ester was observed, resulting in the hydrophobic crosslinks disruption and release of encapsulated Doxorubicin. The increasing release ratio of hydrophobic pharmaceutical Dox due to hydrophobic microstructure disintegration upon irradiation enhanced apoptosis ratio of HeLa cell. With these attractive properties, the photo-responsive injectable hydrogel as presented here may provide new opportunities in a truly physiological environment for site-specific on demand drug release.

Experiment

Materials and methods

p-nitrophenylchloroformate was purchased from Meyer chemical Co Ltd without further purity. *L*-Glutamate acid (Aladdin) was used as received. 1,1,3,3-tetramethylguanidine (TMG, 98%, Aldrich) were distilled under reduced pressure. Tetra-PEG-NH_2 was purchased from Sigma-Aldrich. Dox·HCl and Nile Red were from J&K chemical. N,N-dimethylacetamide (extra dry, with molecular sieves, water≤50 ppm) and *o*-nitrobenzyl alcohol were purchased from Energy Chemical. The HeLa cells were purchased from the Shanghai Institute of Cell Biology (Shanghai, China). Fetal bovine serum (FBS), 4,6-diamidino-2-phenylindole (DAPI), trypsin, phosphate buffered saline (PBS), and Dulbecco's modified Eagle's medium (DMEM) were purchased from GIBCO and used as received. Cell culture lysis buffer, 4',4',6-diamidino-2-phenylindole bromide (MTT) were purchased from Beyotime Institute of Biotechnology (Shanghai, China). All other reagents were purchased from Sinopharm Chemical Reagent Co Ltd. and used as received. Water was deionized with a Milli-Q SPreagent water system (Millipore) to a specific resistivity of 18.4 mΩ cm.

^{1}H NMR (300 MHz) and ^{13}C NMR (75 MHz) spectra were acquired on a 300 MHz Bruker instrument. ESI-MS experiment was performed on Thermo Scientific LTQ Orbitrap Mass Spectrometer equipped with an electrospray interface. Fourier transform infrared (FT-IR) spectra were recorded on a Bruker VECTOR-22 IR spectrometer. Molecular weight and molecular weight distributions, PDI, were determined by gel permeation chromatography (GPC) equipped with a Waters 1515 pump and a Waters 2414 differential refractive index detector (set at 30°C). It used a series of three linear Styragel columns at an oven temperature of 45 °C. The eluent was DMF at a flow rate of 1.0 mL/min. A series of low polydispersity polystyrene standards were employed for calibration. The degrees of polymerization, DPs, ware determined by ^{1}H NMR analysis. UV/vis absorbance was conducted on a double-beam UV-Vis spectrophotometer (Shimadzu). 365nm LED lamp was used for UV irradiation. Fluorescence experiments were conducted on a RF-5301/PC (Shimadzu) fluorospectro photometer. Rheological properties of all prepared hydrogels were studied on a Rheometer (TA instruments, AR-G2) with a platform of 40 mm diameter.

Synthetic procedure

Schematic synthetic procedures are shown in scheme 2, Figure S1.

Synthesis of the N-(*p*-nitrophenoxycarbonyl)-*γ*-*o*-nitrobenzyl-*L*-glutamate (NPNBLG)

NPNBLG was synthesised according to the literature.[41] Briefly, *o*-nitrobenzyl alcohol (1.53 g, 10 mmol, 1.0 equiv.) was dissolved in dichloromethane (30 mL), then phosphorus tribromide (1.05 mL, 1.1 equiv) was added at ice bath. The mixture was then stirred at room temperature and monitored by TLC for 6 h. After that, the reaction mixture was washed with saturated brine, dried over $MgSO_4$, and the solvent was removed under reduced pressure. Then the product was dried overnight in a vacuum oven at room temperature, affording *o*-nitrobenzyl bromide as a yellowish solid for using without further purification.

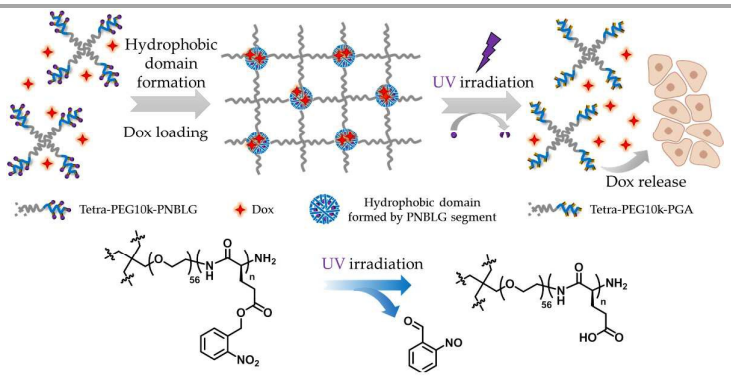

Scheme 1: Schematic illustration of the design and application of the photo-responsive injectable hydrogel.

View Article Online
DOI: 10.1039/C8SM01575A

In a 250-mL round bottom flask, *N*,*N*,*N'*,*N'*-tetramethylguanidine (11 mL, 87 mmol) was added slowly to a stirred *L*-glutamic acid and *L*-glutamic acid copper (II) complex (30.8 g, 86 mmol) in DMF (40 mL) and distilled water (6 mL). The mixture turned to dark blue. After all solids were dissolved (~2h), additional DMF (31 mL) was added. Then, *o*-nitrobenzyl bromide (25 g, 90 mmol) was added to the above solution in one portion. The reaction solution became darker and was kept at 40 °C for 38 h. After that, acetone (500 mL) was added to the mixture and stirred until a fine precipitate was obtained (~1 h). The violet solid was collected by filtration, followed by addition of freshly prepared EDTA (20 g)/sodium bicarbonate (10 g) aqueous solution (150 mL) and further stirring for 24 h. The product was collected by filtration and washed with DI water. Further purification was performed by recrystallizing from H_2O/isopropanol. Obtained 15.1 g (yield: 49%) ^{1}H NMR [D_2O/DCl (1wt%), δ, ppm]: 8.03 (d, 1H), 7.65 (t, 1H), 7.48~7.55 (m, 2H), 5.39 (s, 2H), 4.05 (t, 1H), 2.65 (t, 2H), 2.18 (m, 2H).

To a solution of *γ*-*o*-nitrobenzyl-*L*-glutamate (2.82 g, 10 mmol) in THF (50 mL), *p*-nitrophenylchloroformate (2.03 g, 10 mmol) was added at room temperature and the mixture was stirred at 40 °C for 24 h. The solvent was removed under reduced pressure, 50 mL DCM was added. Then the solution was washed with distilled water and a saturated NaCl aqueous solution, dried over anhydrous $MgSO_4$, filtered and concentrated by a rotary evaporator. The resulting solid residue was fractionated by column chromatography using a mixed solvent of ethyl acetate/n-hexane (1/1 v/v) to obtain NPNBLG as a white solid (1.6 g, Yield: 35%) ^{1}H NMR [CD_3OD, δ, ppm]: 8.26 (d, 2H), 8.11 (d, 1H), 7.70-7.60 (m, 3H), 5.52 (s, 2H), 4.32 (m, 1H), 2.65 (t, 2H), 2.35 (m, 1H) 2.10 (m, 1H).

Synthesis of the N-(*p*-nitrophenoxycarbonyl)-*γ*-benzyl-*L*-glutamate (NPBLG)

To a solution of *γ*-benzyl-*L*-glutamate (2.37 g, 10 mmol) in THF (50 mL), *p*-nitrophenyl chloroformate (2.03 g, 10 mmol) was added at room temperature and the mixture was stirred at 40 °C for 24 h. The resulting mixture was washed with distilled water and a saturated NaCl aqueous solution, dried over anhydrous $MgSO_4$, filtered, and concentrated by a rotary evaporator. The resulting solid residue was fractionated by column chromatography using a mixed solvent of ethyl acetate/n-hexane (1/1 v/v) to obtain NPBLG as a white solid (1.4 g, Yield: 35%). ^{1}H-NMR [CD_3OD, δ, ppm]: 2.13–2.45 (m, 2H), 2.62 (m, 2H), 4.48–4.56 (m, 1H),F 5.16 (s, 2H), 6.02 (d, 1H), 7.30–7.34 (m, 2H), 7.37 (m, 5H), 8.25 (m, 2H).

Synthetic and characterization of the polymer

Typically, a solution of NPNBLG (0.448 g， 1.0 mmol) and tetra-PEG-NH_2(0.4 g, 0.04 mmol) in N,N-dimethylacetamide (1 mL) was stirred at 60 °C for 48 h under nitrogen. The reaction mixture was poured into an excess of ether for three times, and dried in vacuum oven at room temperature, yielding a solid powder star poly(ethylene glycol)-*b*-poly(*γ*-*o*-nitrobenzyl-*L*-glutamate) (0.52 g, Yield: 74%).

Monomer conversion and mean degree of polymerization (DP) were determined by ^{1}H NMR. Number-average molecular weight (Mn) was determined by ^{1}H NMR analysis, and polydispersity index (PDI, M_w/M_n) was quantified by gel permeation chromatography.

Hydrogel preparation

The hydrogel was prepared by dispersing star PEG-polypeptide conjugates in water. The obtained solutions were gently heated and vigorous stirred for a few minutes to ensure complete dissolution. The solutions were then cooled to room temperature to allow gelation.

Rheological measurements of the hydrogels

Rheological properties of all prepared hydrogels were studied on a Rheometer (TA instruments, AR-G2) with a platform of 40mm diameter. The frequency-sweep measurement was conducted in a constant-strain (0.5%) mode over the frequency range of 0.1-100 rad·s^{-1} at 37°C. Before study the self-healing property, a strain-sweep measurement was conducted at a constant frequency of 6.283 rad·s^{-1} over the strain range of 0.1% to 2000% at 37°C. Finally, a strain step cycled between 1% and 800% was performed at 37°C and 6.283 rad·s^{-1}.

The gel to sol transition upon UV light

The frequency-sweep measurement of hydrogel before and after 30 min UV irradiation was carried out to study its light-sensitive gel-sol transition.

Self-assembly of star PEG-polypeptide conjugates and UV-vis absorbance spectra upon UV light

2 mg star PEG-polypeptide conjugates was dissolved in 1 mL 1,4-dioxane, stirred and maintained at a predetermined temperature in a water bath for 25 min. Then, 8 mL PBS buffer (pH 7.4, 10 mM) was slowly injected at an addition rate of 2 mL/h via a syringe pump. After stirring for another 2 h, 1,4-dioxane was removed by dialysis (cellulose membrane, MWCO: 3.5 kDa) against PBS buffer (pH 7.4, 10 mM). Fresh PBS buffer was replaced approximately every ~4 h. The UV-vis evolution of micelles upon UV irradiation (1 mW/cm^2) was recorded at predetermined time intervals.

Preparation of NR-loaded star PEG-polypeptide conjugates micelle and light-triggered release of Nile Red

2 mg star PEG-polypeptide conjugates and 20 μg Nile Red were dissolved in 1 mL 1,4-dioxane , stirred and maintained at a predetermined temperature in a water bath for 25 min. Then, 8 mL PBS buffer (pH 7.4, 10 mM) was slowly injected at an addition rate of 2 mL/h via a syringe pump. After stirring for another 2 h, 1,4-dioxane was removed by dialysis (cellulose membrane, MWCO: 3.5 kDa) against PBS buffer (pH 7.4, 10 mM). Fresh PBS buffer was replaced approximately every ~4 h. The fluorescence evolution of NR-loaded micelles upon UV irradiation (1 mW/cm^2) was recorded at predetermined time intervals (λ_{ex} = 550 nm).

Preparation of DOX-loaded hydrogel and controlled released of DOX payload

Typically, 30 mg DOX·HCl was dissolved in 1 mL DMSO and 2 mL triethylamine was then added and stirred at room temperature overnight. After that, 300 mg polymer was added and stirred at ambient temperature for 2 h. The mixtures were then subjected to dialysis against PBS buffer (pH 7.4, 10 mM) for 24 h to remove unloaded DOX and DMSO solvent. The

View Article Online
DOI: 10.1039/C8SM01575A

dialysate was adjusted to predetermined volumes (pH 7.4, 10 mM) by adding PBS buffer. According to a standard calibration curve, the DOX loading efficiencies (LE) and the DOX loading contents (LC) were estimated. For the triggered release of DOX, in a typical release experiment, DOX-loaded hydrogels (500 μL) were transferred to a dialysis cell with a molecular weight membrane (MWCO: 3.5 kDa) and then dialyzed against 9.5 mL of PBS buffer (pH 7.4, 10 mM) at 37°C.

In Vitro Cytotoxicity Measurement.

Cell viability was examined by the MTT assay. HeLa cells were seeded in 96-well plate at a density of 10^4 cells per well in 100 μL DMEM medium with 10% FBS at 37 °C under 5% CO_2 humidified atmosphere. Drug-loaded micelles with or without 30 min UV irradiation (1 mW/cm^2) were then added to target a final concentration of 3.0 g/L. After incubating for 24 h, MTT reagent (in 20 μL PBS buffer, 5 mg/mL) was added to each well, and the cells were further incubated with 5% CO_2 for 4 h at 37 °C. The culture medium in each well was removed and replaced by 150 μL of DMSO. The solution from each well was transferred to another 96-well plate, and the absorbance values were recorded at a wavelength of 490 nm by a microplate reader (Thermo Fisher). The cell viability is calculated to be $A_{490,treated}/A_{490,control} \times 100\%$, where $A_{490,treated}$ and $A_{490,control}$ are the absorbance values in the presence and absence of polymeric micelles, respectively. Each experiment was done in quadruple, and the data were shown as the mean value.

Determination of apoptotic cell death

The apoptotic cell death induced by Dox-loaded micelles was examined via DAPI staining of HeLa cells cultured in glass-bottom petri dishes. After treating with and without irradiation Dox-loaded micelles for 24 h, the cells were mixed with DAPI staining solution for each dish. After further incubation for 20 min, the staining solution was removed and washed three times with PBS buffer media. Cell nuclei were stained by DAPI and observed under a confocal laser scanning microscopy using a 405 nm laser. The emission detection channel was set at 440-480 nm.

Results and discussion

Synthesis and characterization of star PEG-polypeptide conjugates

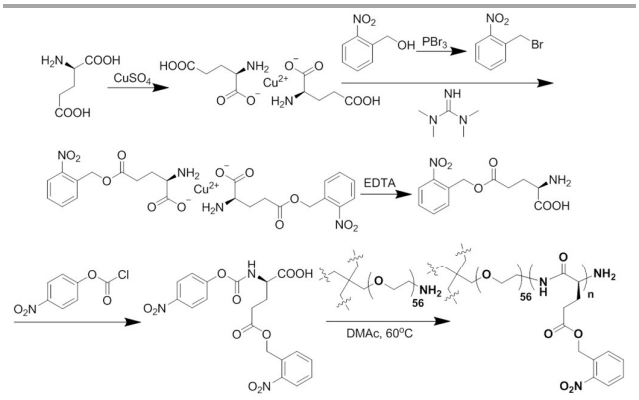

Scheme 2: The synthetic route of star PEG-polypeptide conjugates was shown.

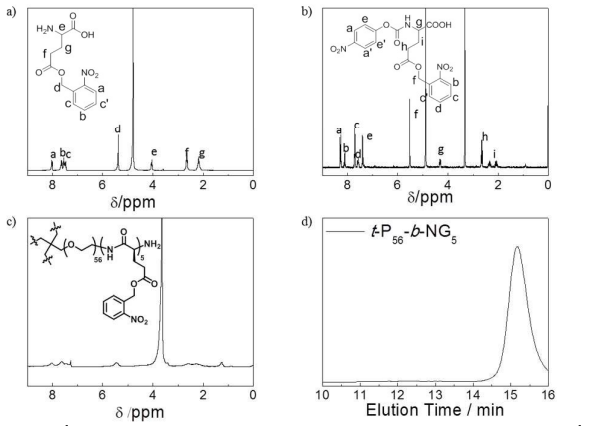

Figure 1: (a) ^{1}H NMR of *γ*-*o*-nitrobenzyl-*L*-glutamate in D_2O with a drop of DCl. (b) ^{1}H NMR of *N*-(*p*-nitrophenoxycarbonyl)-*γ*-*o*-nitrobenzyl-*L*-glutamate in CD_3OD. (c) ^{1}H NMR of amphiphilic diblock copolymers *t*-P_{56}-*b*-NG_5 in $CDCl_3$. d) The GPC trace recorded for amphiphilic diblock copolymer *t*-P_{56}-*b*-NG_5 by DMF elution.

Table 1: The structural parameters of star PEG-polypeptide conjugates.

Star PEG-polypeptide	abbreviation	Mn/kDa[a]	Mw/Mn[b]
t-PEG_{56}-*b*-$PNBLG_5$	*t*-P_{56}-*b*-NG_5	15.6	1.07
t-PEG_{56}-*b*-$PNBLG_7$	*t*-P_{56}-*b*-NG_7	17.9	1.05
t-PEG_{56}-*b*-$PNBLG_{10}$	*t*-P_{56}-*b*-NG_{10}	21.3	1.03
t-PEG_{56}-*b*-$PNBLG_{12}$	*t*-P_{56}-*b*-NG_{12}	23.5	1.08
t-PEG_{56}-*b*-$PNBLG_{15}$	*t*-P_{56}-*b*-NG_{15}	26.9	1.07

[a]Determined by ^{1}H NMR analysis. [b]Obtained from GPC analysis using DMF as eluent.

The star PEG-polypeptide conjugates were synthesised using a novel method according to previously reported work.[48] As shown in Scheme 2, *N*-(*p*-nitrophenoxycarbonyl)-*γ*-*o*-nitrobenzyl-*L*-glutamate, which was prepared by *N*-carbamoylation of *γ*-*o*-nitrobenzyl-*L*-glutamate(Figure 1a and 1b), underwent successful polycondensations with tetra-PEG-NH_2 as initiator to obtain a solid powder star poly(ethylene glycol)-*b*-poly(*γ*-*o*-nitrobenzyl-*L*-glutamate), PEG-polypeptide conjugates.

A series of PEG-polypeptide conjugates were synthesized. Monomer conversion and mean degree of polymerization (DP) were determined by ^{1}H NMR from the ratio of the characteristics of *o*-nitrobenzyl ester moiety at 5.5 ppm and the characteristics of the PEG moiety at 3.5 ppm (Figure 1c and Figure S4). Number-average molecular weight (Mn) was determined by ^{1}H NMR analysis, and polydispersity index (PDI) was quantified by gel permeation chromatography (Figure 1d and Figure S5). A summary table was shown in Table 1.

Rheological characterization of hydrogel

Table2: The mechanical properties of hydrogel of different composition and concentrations.

Weight percent/%	10		20		30	
Entry	G'/kPa	G''/kPa	G'/kPa	G''/kPa	G'/kPa	G''/kPa
t-P_{56}-*b*-NG_5	0.17	0.19	0.85	0.53	1.76	0.77
t-P_{56}-*b*-NG_7	0.55	0.31	4.33	0.93	7.25	1.18
t-P_{56}-*b*-NG_{10}	0.71	0.25	6.30	1.35	11.01	1.65
t-P_{56}-*b*-NG_{12}	0.85	0.28	8.60	2.42	15.46	2.86
t-P_{56}-*b*-NG_{15}	0.96	0.28	10.49	2.65	19.93	4.89

The mechanical properties of hydrogel were carried out on a rotated rheometer.

View Article Online
DOI: 10.1039/C8SM01575A
Journal Name ARTICLE

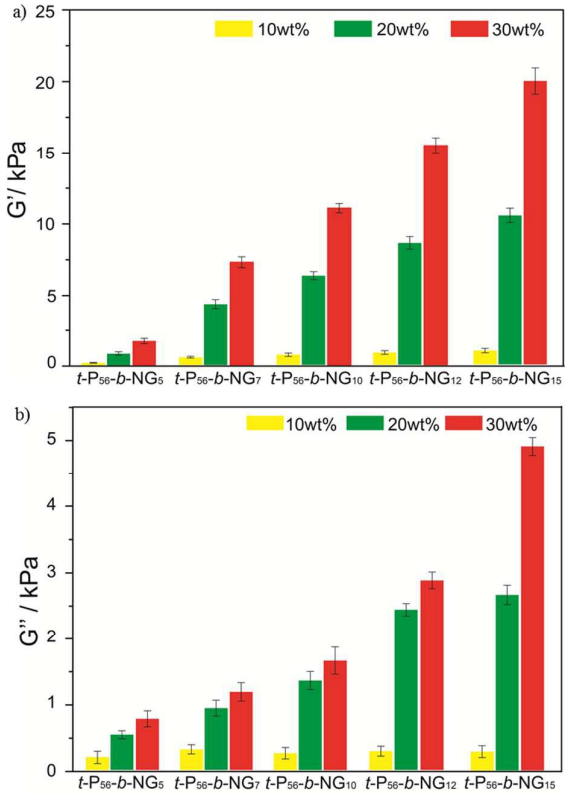

Figure 2: Rheology of star PEG-polypeptide conjugates of hydrogel. (a) Storage modulus (G'/kPa) and (b) Loss modulus (G''/kPa) of hydrogel at different composition and concentration.

To quantify the mechanical properties of star PEG-polypeptide conjugates, a series of hydrogels with different compositions and concentrations were prepared. The frequency sweep measurement of them was performed (Figure S7). All samples formed elastic gels over a broad frequency range except 10 wt% *t*-P_{56}-*b*-NG_5 sample, likely because low hydrophobic content in this sample could not support its weight. The storage modulus and loss modulus of hydrogels increased with increasing star PEG-polypeptide conjugates concentration (Table 2), following trends similar to the previous report.[44] And the corresponding intuitive results were shown in Figure 2.

The mechanical properties of hydrogel similar to surrounding tissue can maintain the integrity of hydrogel under tissue squeezing. The storage modulus of diseased mammalian tissues and organs, such as premalignant breast and fibrotic liver was usual in ~1.6 kPa~2.2 kPa.[49] Therefore, we chose 30 wt% *t*-P_{56}-*b*-NG_5 hydrogel for the next experiments due to approximate storage modulus.

Self-healing and injectable properties of hydrogels

Hydrogels with a self-healing ability will extend thier serviceable range and lifespan. To investigate the mechanical properties regarding shear-thinning and recovery, we performed rheological tests on 30 wt% *t*-P_{56}-*b*-NG_5 hydrogel. A strain sweep measurement was conducted first to figure out the linear viscoelastic region and the gel-sol transition point. As shown in Figure 3a, storage modulus (G') and loss modulus (G'') remained constant during strain increase from 0.1% to 400%, and the value of G' was much larger than that of G'', suggesting that the hydrogel could withstand the deformation at 37 °C. While the strain kept increasing beyond 400%, both G' and G'' dramatically went down, and showed a crossover at strain γ=410%. This indicated that severe slippage of polymer chains appeared and the hydrogel network was disrupted into a sol state. This excellent shear-thinning property of the prepared hydrogel makes it possible to be injected with a springe (Figure 3a inset).

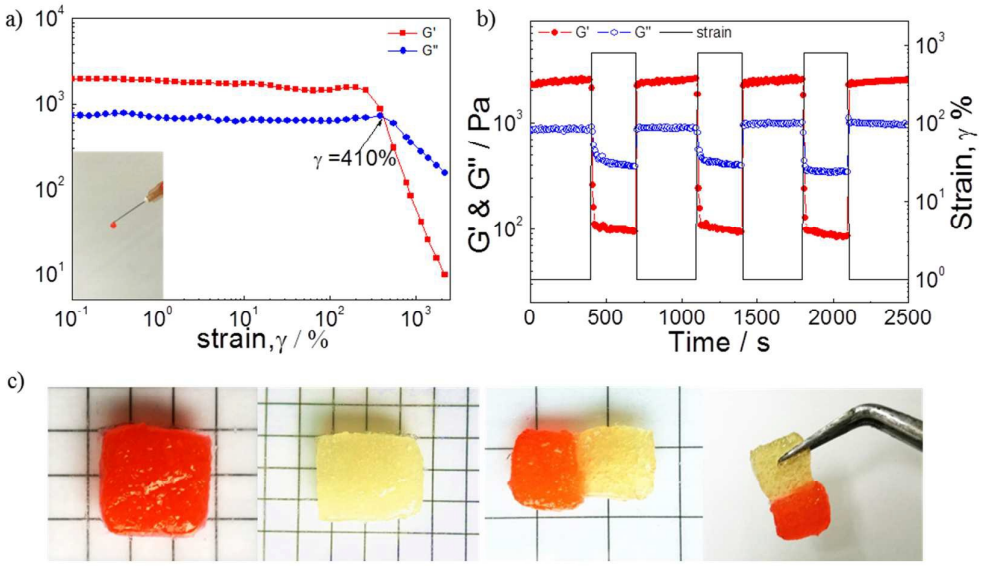

Figure 3: (a) Strain-sweep measurements of a 30 wt% *t*-P_{56}-*b*-NG_5 hydrogel at 37 °C (inset: injection test of the hydrogel stained with Eosin Y at room temperature). (b) Repeated dynamic strain step tests (γ=1 % or 800 %). (c) Separated pieces of hydrogel (stained with Eosin Y and without dye, respectively) were brought together and then self-healing process occurred within 5 min, and the healed hydrogel could support its own weight.

View Article Online
DOI: 10.1039/C8SM01575A

Then, the self-healing was measured by repeated dynamic strain step tests (γ=1% or 800%). The results were shown in Figure 3b, when subjected to 800% strain, the G' of the hydrogel dropped from 2.5 kPa to 0.1 kPa immediately and became smaller than G'' in value, indicating that the hydrogel was disrupted and subsequently transformed into a sol state. After decreasing the strain back to 1%, G' and G'' almost recovered immediately to their initial values, which demonstrated the self-healing capability of the hydrogel. The recovery behavior was relatively fast and completely reversible over the cyclic tests. The self-healing ability of the hydrogel was further demonstrated visually in Figure 3c. A uniform sample was cut into two pieces (one stained with Eosin Y, the other without), and after putting back together, these two hydrogel fragments could adhere and self-repair into one integral piece.

Photograph and rheological studies on gel to sol upon UV irradiation

The photo degradation of the freshly prepared hydrogel in vial was researched. Before UV irradiation, hydrogel in vial couldn't flow (Figure 4a). And the frequency-sweep measurement of hydrogel shown(Figure 4c) that G' was larger than G'', indicating the sample was in gel state. After 30 min UV irradiation, the gel degraded to a fluidic solution (Figure 4b). Meanwhile, the colour of the hydrogel transformed from pale yellow to dark red. The frequency-sweep of the sample after UV irradiation was shown in Figure 4d, G'<G" over the entire frequency range, suggesting the sample was in sol state. The value of G' and G'' after UV irradiation decreased sharply (~90%), indicating that original interaction between chains had been destroyed.

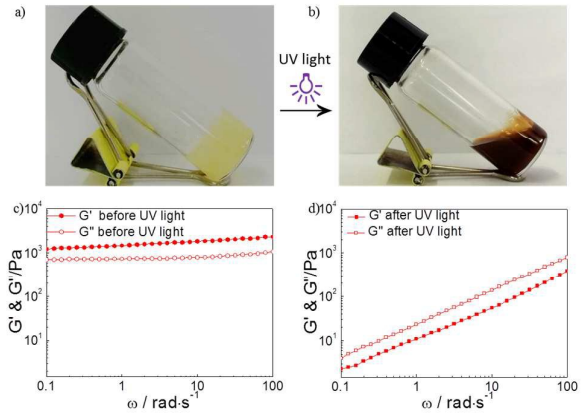

Figure 4: Photographs of the reversed vial test before (a) and after (b) 30 min UV irradiation at 37°C. Frequency-sweep measurement of hydrogel was performed before (c) and after (d) 30 min UV irradiation at 37°C.

Spectroscopy analysis

To verify the degradation mechanism of hydrogel upon UV irradiation, the aqueous micellar solution (0.2 g/L, 25°C) was irradiated with UV light and the kinetics of photochemical reaction was monitored by UV-vis absorption measurements. As shown in Figure 5a, the decrease in number of *o*-notrobenzyl groups is reflected by the decreasing absorption around 265 nm, while the increase of the amount of nitrosobenzaldehye is indicated by its growing absorption around 310 nm. This is in agreement with previous literature reports.[50] The transformation from hydrophobic *o*-nitribenzyl ester to hydrophilic carboxyl derivative increased the dissolution of conjugates.

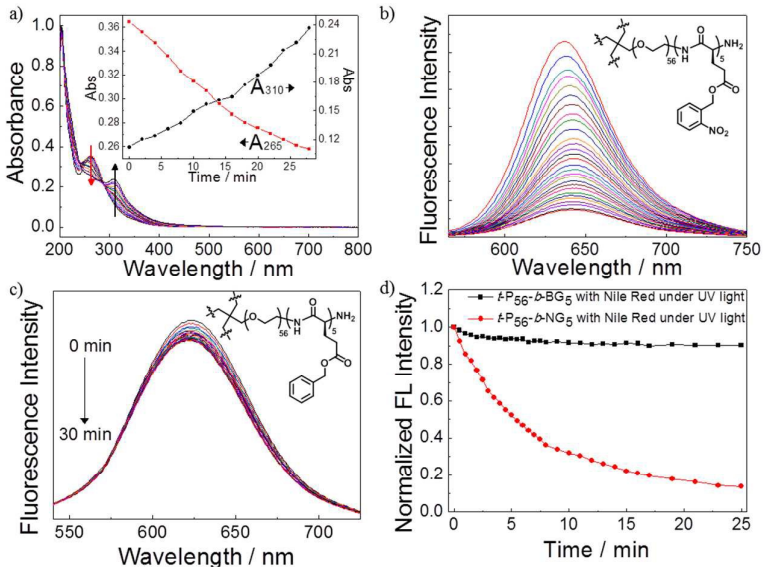

Figure 5: (a) Irradiation time-dependent evolution of UV-vis absorption spectra recorded for the micellar dispersion of *t*-P_{56}-*b*-NG_5 (0.2 g/L, pH 7.4 PBS buffer,25°C). (b) Time-dependent evolution of fluorescence emission spectra of NR-loaded *t*-P_{56}-*b*-NG_5 micellar dispersion (0.2 g/L, pH 7.4 PBS buffer,25°C) upon UV irradiation. (c) Time-dependent evolution of fluorescence emission spectra of NR-loaded *t*-P_{56}-*b*-BG_5 micellar dispersion (0.2 g/L, pH 7.4 PBS buffer,25°C) upon UV irradiation. (d) Normalized emission intensities recorded for NR-loaded *t*-P_{56}-*b*-NG_5 and NR-loaded *t*-P_{56}-*b*-BG_5 micellar dispersion upon UV irradiation.

View Article Online
DOI: 10.1039/C8SM01575A

To further explore the disruption degree of hydrophobic microstructural upon UV irradiation, we utilized Nile Red as a polarity-sensitive fluorescence probe, as it is well-known that Nile Red emission was quenched in water. Evolution of fluorescence emission spectra (λ_{ex}= 550 nm) of Nile Red loaded *t*-P_{56}-*b*-NG_5 micelles (0.2 g/L, 25°C) in PBS buffer (pH 7.4) upon UV irradiation was shown in Figure 5b. The fluorescence intensity of Nile Red exhibited a progressive fluorescence drop and then reached 14% of initial state after 30 min irradiation. In contrast, no distinct changes were observed in emission intensity for the Nile Red loaded without photolabile group *t*-P_{56}-*b*-BG_5 micellar solution after 30 min UV irradiation (Figure 5c), indicating that the influence of photo bleaching was sufficiently low. The true reason for the reduction of fluorescence intensity was that photocleavage of *o*-nitribenzyl ester linkages upon UV irradiation completely disrupted the hydrophobic microstructural.

Photo-regulated Doxorubicin release profile and cytotoxicity of Drug-loaded micelles

The Dox concentrations in the dialysate were quantified by measuring the absorption intensities at 480 nm against corresponding standard calibration curves (Figure S6), and drug LC% was determined to be 4.3% and the LE% was estimated to be approximately 45%. Figure 6a showed the cumulative Dox release profiles from drug-loaded hydrogel under varying conditions. At 37°C and in pH 7.4 buffer solution, ~10% of loaded drug can be released over 24 h for hydrogel without UV irradiation. Whereas, the released rate of Dox significantly accelerated after UV irradiation, caused ~80% release of loaded drug in 24 h.

Next, we examined the cytotoxicity of *t*-P_{56}-*b*-NG_5 micelles in vitro cell via the MTT assay against HeLa cells (Figure 6b). The cell viability of drug-free blank micelles with and without UV irradiation remained to be ~85% at 3.0 g/L polymer concentration, suggesting that PEG-polypeptide conjugates micelles were almost noncytotoxic. When HeLa cells were incubated with Dox-loaded micelles without UV irradiation, ~59% cells survived at 3.0 g/L polymer concentration. The cytotoxicity results can be rationalized by highefficiency of cellular uptake, ester hydrolysis and triggered drug release under cellular enzymes and pH gradients environment. Dox-loaded micelles after 30 min UV irradiation were added to cells culture medium, the cell viability decreased further and only 39% cells survived. Indicating that Dox-loaded micelles subjected to UV irradiation exhibited enhanced treatment performance. The statistically significance difference could be confirmed by Students test with $p < 0.05$. This is also in agreement with the discrepancy in drug release profiles for nonirradiated and irradiated micellar dispersions (Figure 6a). We further assessed the cytotoxicity of the nitrobenzyl alcohol leaving group against HeLa cells (Figure S9), which showed negligible toxicity toward cells.

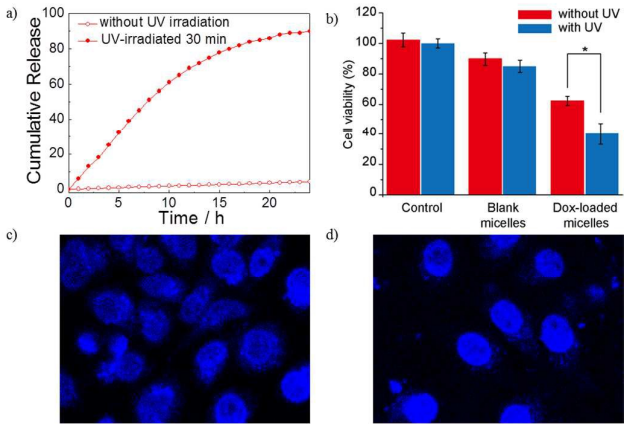

Figure 6: (a) Cumulative Dox release profile from drug-loaded hydrogel (pH 7.4 buffer, 37°C) without and with UV irradiation for 30 min. (b) Comparison of MTT cytotoxicity assay results of blank and Dox-loaded micellad solution of *t*-P_{56}-*b*-NG_5 at a concentration of 3.0 g/L without irradiation (red bar) and with 365 nm UV irradiation (blue bar) against HeLa cells. The data are expressed as mean ± sd (n = 3). *P < 0.05 (*t*-test). Dox-loaded micelles induced apoptosis of HeLa cells as detected by DAPI nuclear staining (405 nm excitation; 440-480 nm blue channel). CLSM images of HeLa cells after incubation for 24 h in the presence of drug-loaded micelles without (c) and with (d) 365 nm UV irradiation for 30 min.

This conclusion was further proved via the DAPI nuclear stain technique. Figure 6c showed CLSM images recorded for HeLa cells after incubation for 24 h in the presence of Dox-loaded micelles without (Figure 6c) and with (Figure 6d) 30 min of UV irradiation. For cells treated with 30 min irradiation, the cell viability was lower, which agreed with the MTT assay results (Figure 6b).

Conclusions

Here, we perpared a photo-degradable injectable self-healing hydrogel based on star poly(ethylene glycol)-*b*-poly(*γ*-*o*-nitrobenzyl-*L*-glutamate) by hydrophobic interactions. The reversible hydrophobic interactions endowed hydrogels with injectable and self-healing properties. Upon photo irradiation, full cleavage of the *o*-nitrobenzyl ester was observed, resulting in a complete hydrogel disruption and controlled release of hydrophobic pharmaceutical. The increasing release ratio of hydrophobic pharmaceutical Dox upon irradiation enhanced apoptosis ratio of HeLa cell. Notably, the medical applications of UV-responsive hydrogel are limited by the high energy of UV radiation (which is harmful to human tissues) and their insufficient tissue penetration, as well as their absorption by biological component. Although UV light was applied for the present study to trigger the gel-to-sol transition and drug release, *o*-nitrobenzyl ester derivatives have been approved to be responsive to near infrared (NIR) irradiation as well possessing better tissue penetration.[51-53] We expect that the further integration of the current design with NIR cleavable moieties will render the hydrogel with improved tissue penetration and more appropriate for real clinical applications.

Notes and references

View Article Online
DOI: 10.1039/C8SM01575A

1. E. A. Appel, J. del Barrio, X. J. Loh and O. A. Scherman, *Chem. Soc. Rev.*, 2012, **41**, 6195-6214.
2. T. Rossow, S. Hackelbusch, P. van Assenbergh and S. Seiffert, *Polym. Chem.*, 2013, **4**, 2515.
3. M. Zhang, C. C. Song, F. S. Du and Z. C. Li, *ACS Appl. Mater. Interfaces*, 2017.
4. X. Hu, Y. Wang, L. Zhang, M. Xu, W. Dong and J. Zhang, *Carbohydr. Polym.*, 2017, **155**, 242-251.
5. M. K. Nguyen, C. T. Huynh, G. H. Gao, J. H. Kim, D. P. Huynh, S. Y. Chae, K. C. Lee and D. S. Lee, *Soft Matter*, 2011, **7**, 2994.
6. C. J. Kearney and D. J. Mooney, *Nat. Mater.*, 2013, **12**, 1004-1017.
7. J. Li and D. J. Mooney, *Nat. Rev. Mater.*, 2016, **1**, 16071.
8. X. Wu, Y. Wu, H. Ye, S. Yu, C. He and X. Chen, *J. Controlled Release*, 2017, **255**, 81-93.
9. J. Jin, Y. Xing, Y. Xi, X. Liu, T. Zhou, X. Ma, Z. Yang, S. Wang and D. Liu, *Adv. Mater.*, 2013, **25**, 4714-4717.
10. Y. Jiang, J. Chen, C. Deng, E. J. Suuronen and Z. Zhong, *Biomaterials*, 2014, **35**, 4969-4985.
11. L. Yu and J. Ding, *Chem. Soc. Rev.*, 2008, **37**, 1473-1481.
12. D. Y. Ko, U. P. Shinde, B. Yeon and B. Jeong, *Prog. Poly. Sci.*, 2013, **38**, 672-701.
13. L. Latxague, M. A. Ramin, A. Appavoo, P. Berto, M. Maisani, C. Ehret, O. Chassande and P. Barthelemy, *Angew. Chem., Int. Ed.*, 2015, **54**, 4517-4521.
14. C. B. Rodell, J. W. MacArthur, S. M. Dorsey, R. J. Wade, L. L. Wang, Y. J. Woo and J. A. Burdick, *Adv. Funct. Mater.*, 2015, **25**, 636-644.
15. K. Wei, M. Zhu, Y. Sun, J. Xu, Q. Feng, S. Lin, T. Wu, J. Xu, F. Tian, J. Xia, G. Li and L. Bian, *Macromolecules*, 2016, **49**, 866-875.
16. G. M. Pawar, M. Koenigs, Z. Fahimi, M. Cox, I. K. Voets, H. M. Wyss and R. P. Sijbesma, *Biomacromolecules*, 2012, **13**, 3966-3976.
17. G. Zhang, Y. Chen, Y. Deng, T. Ngai and C. Wang, *ACS Macro Lett.*, 2017, 641-646.
18. Z. Tao, K. Peng, Y. Fan, Y. Liu and H. Yang, *Polym. Chem.*, 2016, **7**, 1405-1412.
19. H. Yu, Y. Wang, H. Yang, K. Peng and X. Zhang, *J. Mater. Chem. B*, 2017, **5**, 4121-4127.
20. Z. Li, W. Lu, T. Ngai, X. Le, J. Zheng, N. Zhao, Y. Huang, X. Wen, J. Zhang and T. Chen, *Polym. Chem.*, 2016, **7**, 5343-5346.
21. D. E. Apostolides, T. Sakai and C. S. Patrickios, *Macromolecules*, 2017, **50**, 2155-2164.
22. Y. Wang, H. Yu, H. Yang, X. Hao, Q. Tang and X. Zhang, *Macromol. Chem. Phys.*, 2017, **218**, 1700348.
23. H. Yu, Y. Liu, H. Yang, K. Peng and X. Zhang, *Macromol. Rapid Commun.*, 2016, **37**, 1723-1728.
24. J. Li., X. Ni. and K. W. Leong., *J. Biomed. Mater. Res., Part A*, 2003, **65**, 196-202.
25. E. L. Bakota, Y. Wang, F. R. Danesh and J. D. Hartgerink, *Biomacromolecules*, 2011, **12**, 1651-1657.
26. S. B. Christopher and A. P. Nicholas, *Mater. Res. Soc. Symp. Proc.*, 1994, **331**, 211-216.
27. L. Dong, A. K. Agarwal, D. J. Beebe and H. Jiang, *Nature*, 2006, **442**, 551-554.
28. X. Cheng, Y. Jin, T. Sun, R. Qi, H. Li and W. Fan, *Colloids Surf. B* 2016, **141**, 44-52.
29. H. Wu, S. Liu, L. Xiao, X. Dong, Q. Lu and D. L. Kaplan, *ACS Appl. Mater. Interfaces*, 2016, **8**, 17118-17126.
30. X. Wang, C. Wang, Q. Zhang and Y. Cheng, *Chem. Commun.*, 2016, **52**, 978-981.
31. P. D. Thornton, R. J. Mart and R. V. Ulijn, *Adv. Mater.*, 2007, **19**, 1252-1256.
32. S. Matsumoto, S. Yamaguchi, S. Ueno, H. Komatsu, M. Ikeda, K. Ishizuka, Y. Iko, K. V. Tabata, H. Aoki, S. Ito, H. Noji and I. Hamachi, *Chemistry*, 2008, **14**, 3977-3986.
33. April M. Kloxin, Andrea M. Kasko, Chelsea N. Salinas and K. S. Anseth, *Science*, 2009, 59-63.
34. Y. Yang, J. Zhang, Z. Liu, Q. Lin, X. Liu, C. Bao, Y. Wang and L. Zhu, *Adv. Mater.*, 2016, **28**, 2724-2730.
35. G. Pasparakis, T. Manouras, P. Argitis and M. Vamvakaki, *Macromol. Rapid Commun.*, 2012, **33**, 183-198.
36. D. D. McKinnon, T. E. Brown, K. A. Kyburz, E. Kiyotake and K. S. Anseth, *Biomacromolecules*, 2014, **15**, 2808-2816.
37. A. M. Kloxin, M. W. Tibbitt and K. S. Anseth, *Nat. Protoc.*, 2010, **5**, 1867-1887.
38. I. Tomatsu, K. Peng and A. Kros, *Adv. Drug Delivery Rev.*, 2011, **63**, 1257-1266.
39. M. A. Azagarsamy, D. D. McKinnon, D. L. Alge and K. S. Anseth, *ACS Macro Lett.*, 2014, **3**, 515-519.
40. R. Xing, S. Li, N. Zhang, G. Shen, H. Mohwald and X. Yan, *Biomacromolecules*, 2017.
41. L. Yin, H. Tang, K. H. Kim, N. Zheng, Z. Song, N. P. Gabrielson, H. Lu and J. Cheng, *Angew. Chem., Int. Ed.*, 2013, **52**, 9182-9186.
42. T. J. Moyer, J. A. Finbloom, F. Chen, D. J. Toft, V. L. Cryns and S. I. Stupp, *J. Am. Chem. Soc.*, 2014, **136**, 14746-14752.
43. K. L. Niece, C. Czeisler, V. Sahni, V. Tysseling-Mattiace, E. T. Pashuck, J. A. Kessler and S. I. Stupp, *Biomaterials*, 2008, **29**, 4501-4509.
44. G. E. Negri and T. J. Deming, *ACS Macro Lett.*, 2016, **5**, 1253-1256.
45. S. C. Grindy, M. Lenz and N. Holten-Andersen, *Macromolecules*, 2016, **49**, 8306-8312.
46. M. Shan, C. Gong, B. Li and G. Wu, *Polym. Chem.*, 2017, **8**, 2997-3005.
47. S. N. S. Alconcel, A. S. Baas and H. D. Maynard, *Polymer Chemistry*, 2011, **2**, 1442.
48. Y. Kamei, A. Nagai, A. Sudo, H. Nishida, K. Kikukawa and T. Endo, *J. Polym. Sci., Part A: Polym. Chem.*, 2008, **46**, 2649-2657.
49. I. Levental, P. C. Georges and P. A. Janmey, *Soft Matter*, 2007, **3**, 299-306.
50. Y. Li, Y. Qian, T. Liu, G. Zhang and S. Liu, *Biomacromolecules*, 2012, **13**, 3877-3886.
51. B. Yan, J.-C. Boyer, N. R. Branda and Y. Zhao, *Journal of the American Chemical Society*, 2011, **133**, 19714-19717.
52. B. Yan, J.-C. Boyer, D. Habault, N. R. Branda and Y. Zhao, *Journal of the American Chemical Society*, 2012, **134**, 16558-16561.
53. N. Fomina, C. McFearin, M. Sermsakdi, O. Edigin and A. Almutairi, *Journal of the American Chemical Society*, 2010, **132**, 9540-9542.

View Article Online
DOI: 10.1039/C8SM01575A